Journal of Science and Technology ─ Smart Systems and Devices
Volume 36, Issue 3, September 2026, 019–026

Techno-Economic Evaluation of Hybrid Photovoltaic-Battery Energy Storage Systems-Integrated Energy Trading in a Microgrid-Tied Electric Vehicle Charging Cluster

Muhammad Adnan, Myungchin Kim *

Chungbuk National University, Cheongju, South Korea
**Corresponding author email: mckim@cbnu.ac.kr*

Abstract

A microgrid-connected electric vehicle charging cluster with photovoltaic (PV) generation, battery energy storage systems (BESS) and local energy sharing is evaluated using a proposed techno-economic framework. The suggested system studies the impact of local PV generation, stationary storage and internal energy exchange on grid import, energy export, PV utilization and operating cost. The BESS improves the dispatchability of variable PV generation by storing excess energy and supplying charging demand in the high-price or high-load periods. Internal energy trading allows the surplus energy of hybrid charging stations to support the deficit stations in the vicinity before interacting with the utility grid. Simulation results show that the coordinated operation can reduce dependence on the grid, limit the export of low-value energy, improve the utilization of local renewable energy and reduce the overall operating cost of the charging cluster. The proposed framework therefore provides a practical basis for assessing the economic and technical feasibility of renewable-assisted EV charging cluster sunder different solar, storage, and tariff conditions.

Keywords: BESS, electric vehicle charging station, microgrid, P2P energy, PV, techno-economic analysis.

1. Introduction

The rapid growth of electric vehicles (EVs) is changing the operational and economic requirements of modern distribution networks. Extensive use of EV charging may result in temporally and spatially concentrated demand that may increase feeder loading, transformer stress, voltage deviation, and peak power consumption. In the meantime, more distributed PV increases operational variability, with midday oversupply leading to reverse power flow, voltage rise, and low-value exports. The workplace and commercial fleet vehicles are charged during the daytime when PV is available. However, residential EV charging happens overnight when there is no solar energy. Because of this, night charging depends heavily on the grid, creating technical problems as well as economic opportunities for smart charging systems [1, 2].

Incorporating solar power and battery energy storage systems (BESS) at EV charging stations has proven effective in mitigating these challenges. In such systems, surplus PV energy can be stored during high-generation periods and later dispatched during high-demand or high-tariff intervals. This improves renewable energy utilization, reduces peak grid imports, lowers feeder stress, and decreases the amount of surplus PV power exported at relatively low compensation prices. Beyond simple energy shifting, BESS units can also support peak shaving, voltage regulation, renewable intermittency mitigation, and emergency backup operation [3, 4]. Therefore, PV-BESS assisted EV charging stations are increasingly viewed not only as charging facilities, but also as local energy hubs capable of improving the technical and economic performance of distribution-level microgrids [5].

Recent literature has investigated PV, BESS, EV charging, and peer-to-peer (P2P) energy trading from different perspectives. Several studies have shown that PV-BESS systems can reduce operating costs, improve renewable energy utilization, and enhance the technical performance of microgrids and distribution networks [6, 7]. Other works investigated P2P or bilateral energy trading among prosumers, smart homes, buildings, and microgrids, depicting that local energy exchange can reduce electricity bills, improve the value of renewable generation surplus, and provide mutual economic benefits to both energy sellers and buyers [8, 9]. In addition, earlier techno-economic studies have assessed renewable-energy-based microgrid systems using several key indicators, including operating cost, annual cost, power losses, voltage deviation, system reliability, battery degradation, and carbon emissions [10, 11]. Previous works confirm that the evaluation of distributed renewable energy systems should combine the technical operation with the economic evaluation.

However, most existing studies focus on residential prosumers, buildings, or general microgrids, while P2P energy trading among feeder-connected PV-BESS EV charging stations remains less explored. Such clusters have high, concurrent loads and stronger grid impacts, creating opportunities to share local PV surplus instead

p-ISSN 3093-3285
e-ISSN 3093-3315
https://doi.org/10.51316/jst.192.ssad.2026.36.3.3
Received: Jul 3, 2026; Revised: Aug 20, 2026;
Accepted: Sep 3, 2026; Online: Sep 14, 2026

of exporting it at low prices while neighboring stations import at higher tariffs.

Therefore, this paper evaluates PV-BESS-based energy trading in a microgrid-tied EV charging cluster comprising hybrid PV-BESS and conventional grid-dependent stations. Grid-only, isolated PV-BESS, and coordinated P2P trading strategies are compared in terms of operating cost, grid import/export, PV utilization/curtailment, and P2P energy exchange. The framework is further tested under diverse EV charging patterns, including workplace, residential-overnight, and commercial-fleet profiles. Additional analyses evaluate the effects of solar conditions, EV mobility patterns, tariff spread, and grid-export constraints on the economic and operational performance of the proposed framework.

2. Proposed System Architecture

2.1. Electric Vehicle Charging Cluster Topology

The suggested framework consists of a microgrid-tied EV charging cluster connected to a common distribution feeder and point of common coupling (PCC) as illustrated in Fig. 1. The implemented cluster contains three conventional or dumb grid-dependent EV charging stations (D-EVCs) and three hybrid EV charging stations (H-EVCs). Each station contains three 50-kW DC fast chargers and three 7-kW AC slow chargers, giving a maximum connected EV charging powerof 171 kW per station and 513 kW for each three-station class. D-EVCs contain no local generation or storage. Each D-EVC contains only grid-connected EV chargers and has no local PV or BESS. Each station has a maximum connected EV charging power of 171 kW; therefore, the three D-EVCs provide an aggregate maximum EV charging power of 513 kW.

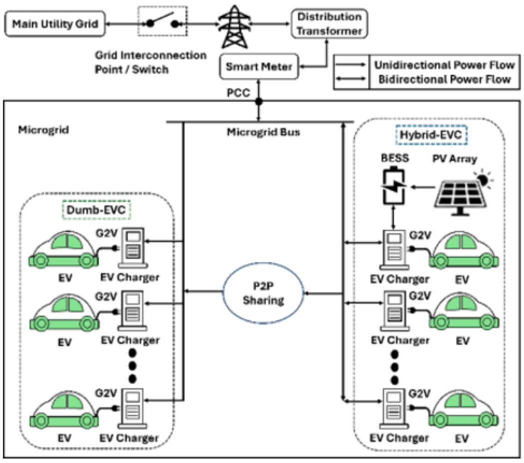

Fig. 1. Proposed EV charging station cluster

Each H-EVC has the same charging infrastructure as a D-EVC but additionally includes local PV generation, BESS, and bidirectional converter capability. This distinction enables H-EVC surplus to support D-EVC demand through the secondary energy management system (SEMS), while the primary energy management system (PEMS) retains station-level power-balance, SoC, and converter constraints. Moreover, each H-EVC is equipped with a 330-kWp PV system interfaced through a 363-kVA PV inverter and a 480-kWh/360-kW lithium-ion BESS connected through a 363-kVA bidirectional converter. For the three H-EVCs, this corresponds to a total installed PV capacity of 990-kWp, a combined BESS energy capacity of 1.44 MWh, and an aggregate maximum BESS charging/discharging power of 1.08 MW. The associated PV inverters and BESS converters each provide an aggregate installed rating of 1.089 MVA. In addition, each H-EVC has a maximum connected EV charging power of 171 kW, resulting in an aggregate maximum EV charging power of 513 kW for the three H-EVCs. The proposed control architecture consists of two coordinated levels: the Primary Energy Management System (PEMS) at the station level and the Secondary Energy Management System (SEMS) at the cluster level. P2P energy sharing and settlement are coordinated within the SEMS and therefore do not constitute a separate control layer.

Table 1. Station configurations

Parameters	D-EVC per station	H-EVC per station
Fast chargers (DC)	3×50 kW	3×50 kW
Slow chargers (AC)	3×7 kW	3×7 kW
Max. station load	171 kW	171 kW
Max. PV system	—	330 kW
PV panel area	—	≈ 1560 m²
PV inverter rating	—	363 kVA
BESS energy capacity	—	480 kWh
BESS power rating	—	360 kW
BESS converter rating	—	363 kVA
BESS round-trip efficiency	—	≈ 0.90
BESS charge/discharge eff.	—	≈ 0.95/0.95
Charger efficiency	≈ 0.92	≈ 0.92

2.2. Role of Photovoltaic, Battery Energy Storage Systems and Peer-To-Peer Trading

The PV system is the primary renewable source at each H-EVC station and is first used to supply local EV charging demand. When PV generation exceeds the instantaneous demand, the available surplus can charge the BESS subject to its power and SoC limits. The stored energy is then dispatched during high-demand or high-price periods, thereby improving local PV utilization, reducing grid dependence, and limiting unnecessary curtailment or low-value exports.

The P2P framework scales flexibility to the broader cluster level. Consequently, H-EVCs with surplus energy can meet the power deficits of D-EVCs before relying on additional grid imports. The internal P2P price is maintained between the SMP export price and the applicable retail ToU price, providing an economic benefit to both sellers and buyers. In real-time operation, P2P trading requires proper metering, communication, billing, and grid connections. To reflect practical grid interaction, the simulation imposes a configurable grid-export window and a maximum PCC export-capacity limit. Specifically, maximum allowable exports are controlled by a set time window and a maximum power limit at the PCC.

3. Mathematical Model

3.1. Photovoltaic-Battery Energy Storage Systems Model

At each H-EVC station, hourly solar-resource and ambient-temperature data are obtained from PVGIS [12]. However, Global Solar Atlas [13] is used for comparison of the site solar-resource conditions for Cheongju, Republic of Korea, and Multan, Pakistan. These data are used as mission-profile inputs for evaluating PV generation, converter loading, and BESS operation [14]. The 2020 dataset contains 8784 hourly samples for each location, which are converted from UTC to the corresponding local standard time to ensure consistent alignment with EV demand, tariff periods, and grid-export constraints. Cheongju provides an annual irradiation of 1724.15 kWh/m² and a modeled PV energy yield of 452.80 MWh per H-EVC, whereas Multan provides 2257.33 kWh/m² and 551.36 MWh, respectively. Thus, Multan exhibits approximately 30.9% higher annual irradiation and 21.8% higher modeled PV generation. However, its higher ambient temperature, with an annual mean of 25.48 °C and a maximum of 45.60 °C, partially offsets the benefit of the greater solar resource. Fig. 2 compares the monthly irradiation, mean ambient temperature, and modeled PV energy for the two locations.

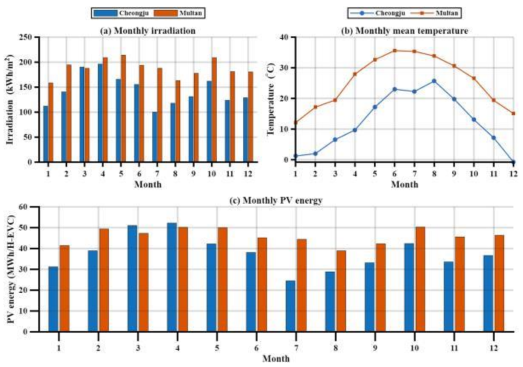

Fig. 2. Yearly Cheongju and Multan solar-resource profiles:(a) irradiation, (b) mean temperature, and (c) PV energy

For each H-EVC station, the BESS SoC is updated using the discrete-time energy balance model [15] in (1). In this formulation, $PB_{ch}(t) \geq 0$, $PB_{dch}(t) \geq 0$ represent the BESS charging and discharging power at time t, respectively. The parameters $\eta ch = \eta dch = 0.95$ are the BESS charge and discharge efficiencies, corresponding to an approximate round-trip efficiency of 0.90 as stated in Table 1 whereas Δt=1h is the dispatch interval. Charging and discharging are mutually exclusive within the dispatch interval. The BESS SoC is maintained within the allowable operating ($SoC_{min} \leq SoC_B \leq SoC_{max}$) range with $SoC_{min} = 0.20$ and $SoC_{max} = 0.90$.

$$SoC_B i(t+1) = SoC_B i(t) + \frac{\left[\eta_{ch} PB_{ch} i(t) - \frac{PB_{dch} i(t)}{\eta_{dch}}\right]\Delta t}{B_{nom,i}} \tag{1}$$

In this study, each H-EVC station is equipped with a $B_{nom,i} = 480$ kWh BESS capacity with a maximum charge/discharge power of 360 kW.

3.2. Utility Grid Tariff and Peer-To-Peer Pricing

The retail electricity price is modeled using the EV charging time-of-use (ToU) structure adopted in the simulation. Therefore, the cost of grid energy purchased by station i, and hour t, is calculated using (2).

$$C_g i(t) = P_g^{imp} i(t) \cdot \Delta t[\beta_{ToU}(t) + \beta_{sur}] \tag{2}$$

Where $C_g i(t)$, is the grid electricity cost in Korean Won (KRW), $P_g^{imp} i(t)$ is the imported grid power of station i, and Δt is the dispatch interval. The ToU tariff, $\beta_{ToU}(t)$ is expressed in KRW/kWh, while β_{sur} denotes the additional grid surcharge, including fuel-cost adjustment and environmental charges, taken as 14 KRW/kWh. Thus, the ToU tariff [16, 17], is formulated as (3) in which the off-peak tariff is defined as 73.5 KRW/kWh whereas the on-peak tariff is expressed as 138.8 KRW/kWh.

$$\beta_{ToU}(t) = \begin{cases} 73.5 & (off-peak\ hours) \\ 138.8 & (on-peak\ hours) \end{cases} \tag{3}$$

Energy exported to the grid is settled at the system marginal price β_{SMP}=80 Won/kWh.

$$\beta_{SMP}(t) < \beta_{P2P}(t) < \beta_{ToU}(t) + \beta_{sur} \tag{4}$$

For the coordinated mode, the P2P tariff, $\beta_{P2P}(t)$ as expressed in (4), is introduced that lies between the feed-in rate and the retail rate so that both the seller and the buyer are strictly better off than transacting with the grid [18].

4. Energy Management System (EMS)

The proposed EMS consists of two interacting control levels, with the cluster-level energy management formulated as a mixed-integer linear programming (MILP) problem. The cluster-level SEMS receives the station surplus/deficit states and coordinates P2P transfer, tariff-aware BESS prepositioning, and PCC interaction. Thus, local feasibility remains with the PEMS, while the SEMS performs decisions that require information from multiple stations. The station-level PEMS manages local PVuse, BESS charging/discharging, SoC protection, and station power balance. For the aggregate H-EVC and D-EVC classes, the hourly power balance accounts for grid exchange, EV demand, and P2P transfer, while the H-EVC additionally incorporates PV generation, BESS operation, and PV curtailment. For station i, the PEMS minimizes the station level operating cost over the considered dispatch horizon with Δt = 1h interval. Following standard transactive EMS and operating-cost formulations [4, 5], and the battery degradation model in [19], the station level PEMS minimizes the local operating cost over the dispatch horizon. The objective accounts for grid-energy purchase, grid-export revenue, BESS degradation, and PV curtailment, as formulated in (5) and represented in Korean Won (KRW).

$$J_i^{PEMS} = \sum_{t=1}^{T}\left[C_g\, i(t) - R_{exp} i(t) + +C_{Bdeg} i(t) + C_{cur}\, i(t)\right] \tag{5}$$

$$R_{exp} i(t) = P_g^{exp} i(t) \cdot \beta_{SMP} \cdot \Delta t \tag{6}$$

$$C_{Bdeg}\, i(t) = k_{deg} \cdot |PB_i(t)| \cdot \Delta t \tag{7}$$

$$C_{cur} i(t) = k_{cur} \cdot P_{cur}\, i(t)| \cdot \Delta t \tag{8}$$

Where $C_g i(t)$ is the local grid-import cost defined in (2), and $R_{exp} i(t)$ is the revenue obtained from grid export at the β_{SMP} rate. $C_{Bdeg} i(t)$ is the BESS degradation cost of station i with $k_{deg} = 20$ KRW/kWh being a linear battery-wear coefficient obtained from the cycle-cost model of [19] and $PB_i(t)$ is the BESS charging/discharging power. Since charging and discharging are mutually exclusive within each dispatch interval, $|PB_i(t)|$ represents the corresponding battery energy throughput. Moreover, the term $C_{cur} i(t)$ representsthe PV-curtailment penalty, where $P_{cur}\, i(t)$ is the curtailed PV power and k_{cur} = 90 KRW/kWh is the curtailment penalty coefficient used in the optimization.

To satisfy practical grid-interaction requirements, export availability and PCC capacity are imposed directly as MILP constraints. In the base case, grid export $P_g^{exp} i(t)$, is permitted only from 09:00 to 18:00 local time, with the aggregate exports at the common PCC limited to P^{max} = 363 kW as defined in (9) and (10). Thus, (9) limits the aggregate PCC export to its allowable capacity during the permitted period and enforces zero export at all other times, whereas $\delta_g(t)$. is the binary export-permission variable defined in (10).

$$0 \le \sum_i P_g^{exp} i(t) \le \delta_g(t) P_{CC}^{max} \tag{9}$$

$$\delta_g(t) = \begin{cases} 1, & 09{:}00 \le t < 18{:}00 \\ 0, & otherwise \end{cases} \tag{10}$$

The PEMS first prioritizes local PV utilization by supplying EV charging demand and charging the BESS with available PV surplus, subject to the corresponding SoC, power, and converter constraints. Any remaining surplus ordeficit, togetherwith the BESS operating state and SoC, is communicatedtothe SEMS. The PEMS also schedules BESS charging and discharging in a tariff-aware manner while maintaining local power balance and operational feasibility.

At the cluster level, the SEMS receives the surplus, deficit, and BESS SoC information from the individual stations and coordinates P2P energy exchange, PCC interaction, and BESS prepositioning. Since the station level grid costs, export revenue, BESS degradation, and PV-curtailment terms are already included in J_i^{PEMS}, the SEMS objective aggregates the PEMS costs and adds only the coordination-related terms, as expressedin (11).

$$J^{PEMS} = \sum_{i=1}^{N} J_i^{PEMS} + \sum_{t=1}^{T}\left[C_{PCC,dew}(t) + C_{P2P}(t) + C_{Pre}(t)\right] \tag{11}$$

The PCC-power deviation, $C_{PCC,dev}(t)$ is penalized using the nonnegative auxiliary variable $d(t)$, as expressed in (12).

$$\left.\begin{aligned} C_{PCC,dev}(t) = k_L d(t) \\ -d(t) \le P_g^{net} - \bar{P}_L \le d(t), \quad d(t) \ge 0 \end{aligned}\right\} \tag{12}$$

where k_L is the PCC-power deviation weighting coefficient, P_g^{net} is the net power exchanged at the PCC, and $\bar{P}_L$ is the mean aggregate EV load over the dispatch horizon. The double-sided constraint in (12) represents the absolute deviation of the net PCC power from $\bar{P}_L$ while preserving the linear MILP formulation. In the implemented model, kL = 0.25 KRW/kW. The P2P transaction cost is expressed as (13).

$$C_{P2P}(t) = k_{P2P} \cdot P_{P2P}(t) \cdot \Delta t \tag{13}$$

In (13), $P_{P2P}\,(t)$ denotes the aggregate P2P transfer power and k_{P2P} = 1 KRW/kWh is the transaction-cost coefficient associated with local energy exchange. Moreover, the BESS prepositioning penalty is represented by (14).

$$C_{Pre}(t) = k_{pre} s_{pre}(t) \tag{14}$$

where $s_{pre}(t) \ge 0$represents the BESS prepositioning shortfall, and k_{pre} is its penalty coefficient. The penalty encourages the target to be met whenever feasible. The SEMS therefore acts as the cluster-level supervisory coordinator, while station-level feasibility remains enforced by the PEMS. Surplus H-EVC energy is allocated to deficit D-EVCs before additional grid interaction, while P2P exchange and BESS operation are coordinated to reduce grid dependence and PCC-power deviation subject to the BESS SoC, converter, PCC, and station power-balance constraints. The P2P tariff defined in (4) is used for internal buyer–seller settlement and is bounded between the SMP export price and the applicable retail electricity price. Since buyer payments and seller revenues are internal cluster transfers, only the P2P transaction cost is included in the SEMS objective in (11).

5. Results and Discussion

5.1. Simulation Setup

The study is implemented in MATLAB using the intlinprog solver. Hourly PVGIS data for 2020 are used without synthetic fallback, with timestamps converted to Korea Standard Time (UTC+9) and Pakistan Standard Time (UTC+5). A representative 168-h operating week beginning on day 172 of 2020 (20 June) is considered. To ensure a consistent comparison, the same Korean tariff structure is applied to both Cheongju and Multan, thereby isolating the effects of solar and temperature conditions from location-specific tariff differences. All MILP cases, including the base-case, tariff-spread, export-policy, and EV-mobility analyses, converged successfully. The optimization minimizes the cluster operating cost while accounting for battery degradation, PV curtailment, P2P transactions, feeder-power variation, and deviations from the BESS prepositioning target. The principal equipment ratings are summarized in Table 1, while the tariff, BESS, P2P, and grid-interaction parameters are defined in Sections 3 and 4.

5.2. Solar Resource and Base-Case Performance

Multan shows higher PV availability than Cheongju, with the annual capacity factor increasing from 15.6% to 19.0%. During the representative week, aggregate PV generation reaches 24.9 MWh in Cheongju and 31.2 MWh in Multan.As summarized inTable 2,PEMS Only reduces weekly external operating costs by 18.4% in Cheongju and 21.1% in Multan, while Coordinated P2P increases the savings to 32.9% and 40.7%, respectively. Grid imports are reduced by 28.1% in Cheongju and 35.6% in Multan. Coordinated P2P also eliminates the 5.4 MWh and 7.1 MWh PV curtailment observed under PEMS Only and enables 9.8 MWh and 13.4 MWh of internal P2P exchange, respectively. The greater benefit in Multan is mainly due to its higher PV availability and larger surplus available for local energy sharing.

Table 2. Grid Only / PEMS only / coordinated P2P performance for both locations

Metric	Cheongju	Multan
Grid import	83.5/64.5/60.0	83.5/60.1/53.8
Grid export	0 / 0 / 0.9	0 / 0 / 1.0
P2P trade	0 / 0 / 9.8	0 / 0 / 13.4
PV curtailment	– / 5.4 / 0	– / 7.1 / 0
BESS throughput	– / 11.8 / 10.2	– / 14.1 / 9.7
External net cost	9.9 / 8.1 / 6.7	9.9 / 7.8 / 5.9

Note: Energy quantities are in MWh whereas external net cost is in MKRW

5.3. Tariff-Spread Sensitivity and the Role of Peer-To-Peer

Fig. 3 illustrates that a larger tariff-spread coefficient $k = \beta_{on}/\beta_{off}$ generally enhances the economic benefit of coordinated P2P trade, where β_{on} and β_{off} denote the on-peak and off-peak electricity tariffs, respectively. Thus, alarger k represents a wider peak tooff-peakprice differential. In Fig. 3(a), P2P energy initially increases in Cheongju from approximately 6.9 MWh at k = 1.3 to 9.8 MWh at the base-case $k \approx 1.89$ (vertically dashed line), reaching about 10.8 MWh at k = 2.2. Similarly, Multan increases from about 10.1 MWh to 13.4 MWh due to its greater PV availability. Beyond $k \approx 2.2$, P2P energy remains nearly constant in both locations, indicating that the available local surplus and demand, rather than the tariff spread, become the limiting factors.

In contrast, Fig. 3(b) shows a continued increase in economic benefit as k increases. For Cheongju, the cost saving relative to PEMS Only rises from 15.5% at k = 1.3 to about 18% at the base case and 33% at k = 5.2, whereas Multan increases from about 21.5% to about 25% and 43%, respectively. These results indicate that even after the P2P energy exchange reaches its physical saturation level, a wider tariff spread further improves the economic value of locally coordinated energy sharing by avoiding increasingly expensive on-peak grid purchases.

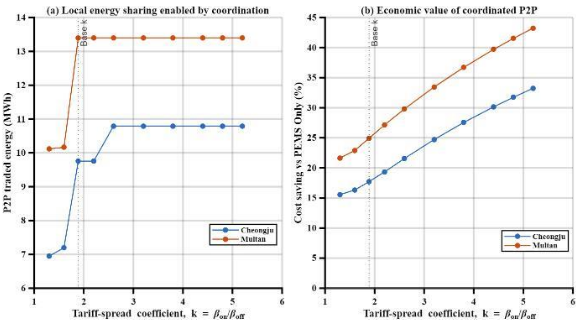

Fig. 3. Effect of the tariff-spread coefficient on (a) P2P traded energy and (b) Coordinated-P2P cost saving

5.4. Weekly Dispatch of Electric Vehicle Stations

The weekly dispatch considers separate aggregate demand profiles for three 171-kW H-EVCs and three 171-kW D-EVCs, giving each class a maximum connected charging capacity of 513 kW. Their differing demand profiles create surplus–deficit periods suitable for P2P exchange. As shown in Fig. 4, PEMS Only uses local PV and BESS but does not allow inter-station energy transfer. Because the MILP enforces import/export exclusivity at the common PCC, H-EVC surplus cannot be exported while D-EVCs are importing and is therefore curtailed. Coordinated P2P instead transfers this surplus to D-EVCs, reducing grid import and curtailment; any remaining surplus is exported, yielding 0.916 MWh of weekly grid export in Cheongju.

The same coordination mechanism is more pronounced in Multan due to its higher PV availability as depicted in Fig. 5. Coordinated P2P increases internal energy exchange to 13.399 MWh, compared with 9.756 MWh in Cheongju, and reduces weekly grid import to 53.778 MWh. The BESS stores surplus PV energy during the day and discharges when demand exceeds supply. Meanwhile, the battery power and SoC remain within their specified operating bounds. These results confirm that the additional economic benefit in Multan is achieved through greater renewable-energy utilization and P2P exchange without violating storage constraints.

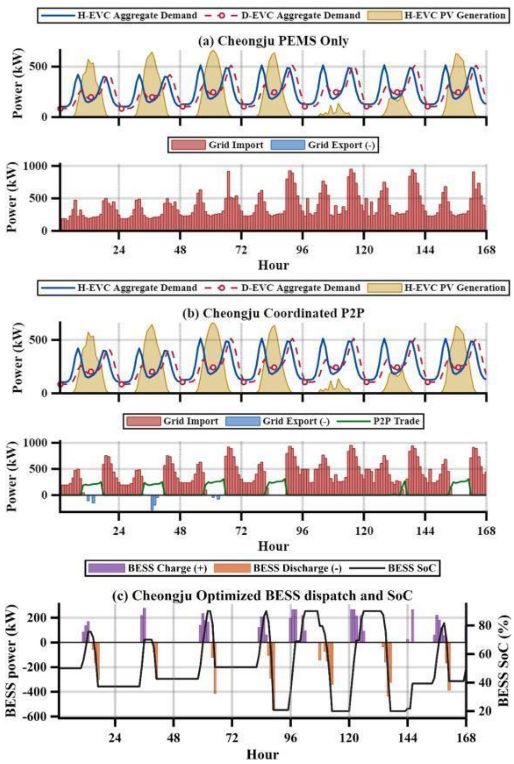

Fig. 4. Cheongju weekly dispatch: (a) PEMS Only, (b) Coordinated P2P, and (c) Optimized BESS dispatch

5.5. Practical Grid-Export Compliance

Both locations comply with prescribed grid-export limits under the coordinated P2P framework as illustrated in Fig. 6. Power export to the grid is allowed within the set window of 09:00–18:00, and no export occurs outside this period, resulting in 0 MWh of night-time export for both Cheongju and Multan. Under the Coordinated P2P case, the total exported energy is limited to 0.916 MWh in Cheongju and 1.004 MWh in Multan. The corresponding maximum hourly export powers are 287.724 kW and 252.926 kW, respectively, both remaining below the configured 363-kW PCC export limit, thereby confirming compliance with the imposed grid-interconnection constraint.

Sensitivity results for the export policy demonstrate that the economic value of this coordination model remains strong even under restricted grid-export conditions. In Cheongju, the external net cost decreases only marginally from 6.676 MKRW when export is disabled to 6.670 MKRW under the configured daytime export limit. Similarly, in Multan, the cost changes from 5.904 MKRW to 5.886 MKRW. These relatively small differences indicate that the principal economic benefit is achieved through local utilization of PV generation, BESS scheduling, and P2P energy exchange to reduce high-cost grid imports, rather than through maximizing revenue from electricity exported to the utility grid.

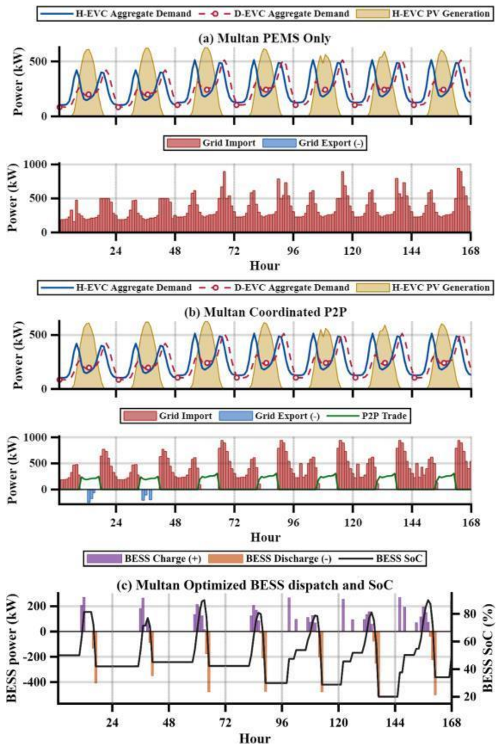

Fig. 5. Multan weekly dispatch: (a) PEMS Only, (b) Coordinated P2P, and (c) Optimized BESS dispatch

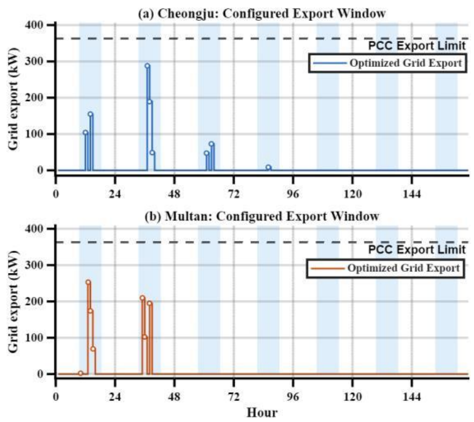

Fig. 6. Grid-export compliance under the configured 09:00-18:00 export window and PCC export limit

5.6. Validation Across Electric Vehicle Mobility Patterns

Variations in EV charging demand are closely tied to mobility patterns, specifically when vehicles arrive and depart. To examine the robustness of the proposed coordination framework under different charging conditions, three representative parametric mobility profiles are considered: workplace charging, residential-overnight charging, and commercial-fleet charging, as illustrated in Fig. 7. Each H-EVC and D-EVC demand profile is normalized to the same 171-kW station rating, while only the time-of-day charging pattern is varied to represent the corresponding mobility behavior. The workplace profile features heavy charging throughout the day. In contrast, residential charging concentrates energy demand in the evening and night. However, commercial fleet profiles create distinct demand peaks based on vehicle operating cycles. The corresponding weekly EV energies are 81.440, 70.631, and 65.017 MWh, respectively. Because the profiles have different energy demands, the analysis compares operating strategies within each profile rather than absolute costs across profiles.

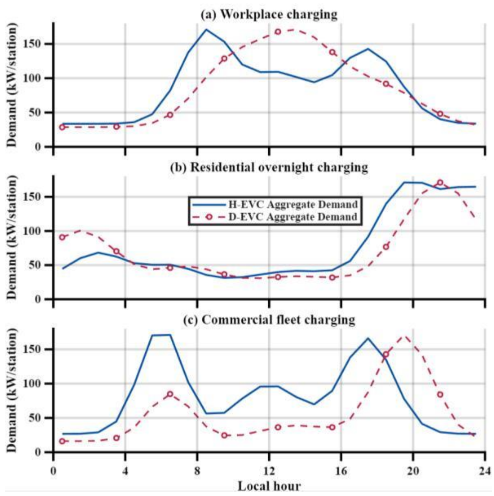

Fig. 7. EV mobility profiles: (a) workplace, (b) residential overnight, and (c) commercial fleet charging

As illustrated in Fig. 8, the Coordinated P2P strategy provides consistent economic benefits under all three EV mobility patterns. Relative to Grid Only, the cost savings in Cheongju are 34.5%, 33.7%, and 39.6% for workplace, residential-overnight, and commercial-fleet charging, respectively, while the corresponding savings in Multan are 42.7%, 40.8%, and 48.5%. Compared with PEMS Only, Coordinated P2P achieves additional savings of 11.4%, 28.8%, and 20.6% in Cheongju and 15.6%, 37.9%, and 29.7% in Multan for the same mobility profiles.

The incremental benefit of P2P coordination is lowest for workplace charging because a larger portion of daytime EV demand coincideswith local PV generation, enabling PEMS Only to utilize more PV directly. In contrast, residential-overnight charging exhibits limited temporal overlap with PV production; therefore, BESS scheduling and inter-station energy exchange provide greater economic value, yielding the highest savings relative to PEMS Only. Commercial-fleet charging contains more concentrated demand intervals, during which coordinated P2P exchange reduces dependence on high-cost grid imports. Across all three profiles, Multan consistently achieves higher savings than Cheongju, primarily due to its greater PV availability and consequently larger amount of energy available for local redistribution.

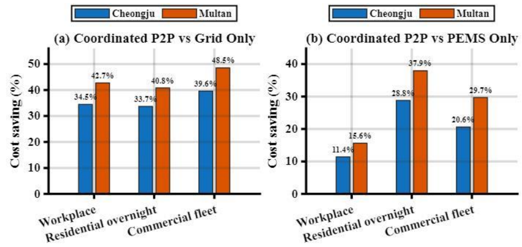

Fig. 8. Coordinated-P2P operating-cost saving across the three EV mobility profiles

5.7. Scope and Limitations

The proposed study broadens the framework evaluation and improves the representation of practical grid interaction but remains a numerical proof-of-concept. Results are based on a representative summer week from PVGIS 2020 and parametric EV mobility profiles rather than measured charger-occupancy data. The feeder is modeled at the aggregate PCC level; detailed AC power flow, protection coordination, communication delays, and converter switching dynamics are excluded. The same Korean tariff is applied to Cheongju and Multan to isolate climatic effects, so Multan represents a climate-comparison case rather than a Pakistan-specific tariff assessment. Battery degradation is represented by alinear energy-throughput cost instead of a nonlinear electrochemical aging model. These limitations motivate future experimental and field validation while preserving comparative conclusions under the stated assumptions.

6. Conclusion

This paper presented a PV-BESS-P2P energy management framework for a grid-connected EV charging cluster comprising three hybrid H-EVCs and three grid-dependent D-EVCs. The proposed two-layer architecture integrates local PEMS operation with coordinated SEMS optimization, where the PEMS manages station-level power balance, PV utilization, BESS dispatch, SoC limits, and local feasibility, while the SEMS coordinates P2P energy exchange and PCC level operation. The MILP formulation further incorporates distinct H-EVC/D-EVC demand profiles, configurable grid-export periods, PCC export-capacity limits, and prevention of simultaneous grid import and export.

Simulation results show that Coordinated P2P consistently improves the cluster techno-economic performance over Grid Only and PEMS Only operation. For the representative week, operating costs decreased by 32.9% in Cheongju and 40.7% in Multan relative to Grid Only, with additional savings of 17.7% and 24.9% over PEMS Only. Coordinated mode reduces grid imports to 60.021 MWh in Cheongju and 53.778 MWh in Multan, enables 9.756 and 13.399 MWh of P2P exchange, respectively, and eliminates the PV curtailment under PEMS Only. The strategy remains effective across diverse EV charging patterns, with greater economic benefit under peak-to-off-peak tariff spreads. Overall, the framework improves renewable utilization, reduces grid dependence, and supports economical and grid-compliant EV charging.

References

[1] M. Ahmed, Y. Abouelseoud, N. H. Abbasy, and S. H. Kamel, Hierarchical distributed framework for optimal dynamic load management of electric vehicles with vehicle-to-grid technology, IEEE Access, vol. 9, pp. 164643–164658, 2021. https://doi.org/10.1109/ACCESS.2021.3134868

[2] E. L. Karfopoulos and N. D. Hatziargyriou, Distributed coordination of electric vehicles providing V2G services, IEEE Trans. Power Syst., vol. 31, iss. 1, pp. 329–338, Jan. 2016. https://doi.org/10.1109/TPWRS.2015.2395723

[3] Z. Liu, J. Tan, W. Guo, C. Fan, W. Peng, Z. Fang, and J. Gao, Hierarchical optimal dispatching of electric vehicles based on photovoltaic-storage charging stations, Mathematics, vol. 12, iss. 21, Oct. 2024, Art. no. 3410. https://doi.org/10.3390/math12213410

[4] IEEE Standard for Interconnection and Interoperability of Distributed Energy Resources with Associated Electric Power Systems Interfaces, IEEE Std 1547-2018, Apr. 2018. https://doi.org/10.1109/IEEESTD.2018.8332112

[5] M. N. Akter, M. A. Mahmud, and A. M. T. Oo, A hierarchical transactive energy-management system for microgrids, in Proc. IEEE Power and Energy Society General Meeting (PESGM), Boston, MA, USA, pp. 1–5, Jul. 2016. https://doi.org/10.1109/PESGM.2016.7741099

[6] C. Long, J. Wu, Y. Zhou, and N. Jenkins, Aggregated battery control for peer-to-peer energy sharing in a community microgrid with PV battery systems, Energy Procedia, vol. 145, pp. 522–527, Jul. 2018. https://doi.org/10.1016/j.egypro.2018.04.076

[7] A. Paudel and H. B. Gooi, A hierarchical peer-to-peer energy trading in community microgrid distribution systems, in 2018 IEEE Power & Energy Society General Meeting (PESGM), Portland, OR, USA, pp. 1–5. Dec. 018. https://doi.org/10.1109/PESGM.2018.8586168

[8] H. Görgülü, Y. Topçuoğlu, A. Yaldız, T. Gökçek, Y. Ateş, and O. Erdinç, Peer-to-peer energy trading among smart homes considering responsive demand and interactive visual interface for monitoring, Sustain. Energy Grids Netw., vol. 29, Mar. 2022, Art. no. 100584. https://doi.org/10.1016/j.segan.2021.100584

[9] N. Spiliopoulos, I. Sarantakos, S. Nikkhah, G. Gkizas, D. Giaouris, P. Taylor, U. Rajarathnam, and N. Wade, Peer-to-peer energy trading for improving economic and resilient operation of microgrids, Renewable Energy, vol. 199, pp. 517–535, Nov. 2022. https://doi.org/10.1016/j.renene.2022.08.061

[10] A. Martín-Crespo, A. Hernández-Serrano, Ó. Izquierdo-Monge, P. Peña-Carro, Á. Hernández-Jiménez, F. Frechoso-Escudero, and E. Baeyens, AC/DC optimal power flow and techno-economic assessment for hybrid microgrids: TIGON CEDER demonstrator, Front. Energy Res., vol. 12, Aug. 2024, Art. no. 1399114. https://doi.org/10.3389/fenrg.2024.1399114

[11] S. Amini, S. Bahramara, H. Golpîra, B. Francois, and J. Soares, Techno-economic analysis of renewable-energy-based micro-grids considering incentive policies, Energies, vol. 15, iss. 21, Nov. 2022, Art. no. 8285. https://doi.org/10.3390/en15218285

[12] European Commission, Joint Research Centre, Photovoltaic Geographical Information System (PVGIS). [Online]. Available: https://joint-research-centre.ec.europa.eu/photovoltaic-geographical-information-system-pvgis_en. Accessed on: Jun. 4, 2026.

[13] World Bank Group, Global Solar Atlas. [Online]. Available: https://globalsolaratlas.info. Accessed on: Jun. 4, 2026.

[14] S. Peyghami, H. Wang, P. Davari, and F. Blaabjerg, Mission-profile-based system-level reliability analysis in DC microgrids, IEEE Trans. Ind. Appl., vol. 55, iss. 5, pp. 5055–5067, Sep.–Oct. 2019. https://doi.org/10.1109/TIA.2019.2920470

[15] K. S. Ng, C.-S. Moo, Y.-P. Chen, and Y.-C. Hsieh, Enhanced coulomb-counting method for estimating state-of-charge and state-of-health of lithium-ion batteries, Applied Energy, vol. 86, iss. 9, pp. 1506–1511, Sep. 2009. https://doi.org/10.1016/j.apenergy.2008.11.021

[16] Korea Electric Power Corporation, Electric rates table: Electric power for EV charging. [Online]. Available: https://home.kepco.co.kr/kepco/indi/foreign/en/html/F/B/ENFBHP00102.html. Accessed on: Jun. 11, 2026.

[17] Korea Power Exchange, Electric Power Statistics Information System, Hourly SMP: System Marginal Price. [Online]. Available: https://epsis.kpx.or.kr/epsisnew/selectEkmaSmpShdGrid.do?locale=eng&menuId=040202. Accessed on: Jun. 11, 2026.

[18] W. Tushar, T. K. Saha, C. Yuen, D. Smith, and H. V. Poor, Peer-to-peer trading in electricity networks: An overview, IEEE Transactions on Smart Grid, vol. 11, iss. 4, pp. 3185–3200, Jul. 2020. https://doi.org/10.1109/TSG.2020.2969657

[19] B. Xu, A. Oudalov, A. Ulbig, G. Andersson, and D. S. Kirschen, Modeling of lithium-ion battery degradation for cell life assessment, IEEE Transactions on Smart Grid, vol. 9, iss. 2, pp. 1131–1140, Mar. 2018. https://doi.org/10.1109/TSG.2016.2578950